ARMY RESEARCH LABORATORY

# Moving Target Indication for Transparent Urban Structures

**by Anthony Martone, Roberto Innocenti, and Kenneth Ranney**

**ARL-TR-4809** **May 2009**

## NOTICES

### Disclaimers

The findings in this report are not to be construed as an official Department of the Army position unless so designated by other authorized documents.

Citation of manufacturer's or trade names does not constitute an official endorsement or approval of the use thereof.

Destroy this report when it is no longer needed. Do not return it to the originator.

**Army Research Laboratory**
Adelphi, MD 20783-1197

**ARL-TR-4809** **May 2009**

# Moving Target Indication for Transparent Urban Structures

**Anthony Martone, Roberto Innocenti, and Kenneth Ranney**
**Sensors and Electron Devices Directorate, ARL**

| REPORT DOCUMENTATION PAGE | Form Approved OMB No. 0704-0188 |
|---|---|



| 1. REPORT DATE *(DD-MM-YYYY)* | 2. REPORT TYPE | 3. DATES COVERED (From - To) |
|---|---|---|
| May 2009 | Final | |

| 4. TITLE AND SUBTITLE | 5a. CONTRACT NUMBER |
|---|---|
| Moving Target Indication for Transparent Urban Structures | 5b. GRANT NUMBER |
| | 5c. PROGRAM ELEMENT NUMBER |

| 6. AUTHOR(S) | 5d. PROJECT NUMBER |
|---|---|
| Anthony Martone, Roberto Innocenti, and Kenneth Ranney | 5e. TASK NUMBER |
| | 5f. WORK UNIT NUMBER |

| 7. PERFORMING ORGANIZATION NAME(S) AND ADDRESS(ES) | 8. PERFORMING ORGANIZATION REPORT NUMBER |
|---|---|
| U.S. Army Research Laboratory<br>ATTN: AMSRD-ARL-SE-RU<br>2800 Powder Mill Road<br>Adelphi, MD 20783-1197 | ARL-TR-4809 |

| 9. SPONSORING/MONITORING AGENCY NAME(S) AND ADDRESS(ES) | 10. SPONSOR/MONITOR'S ACRONYM(S) |
|---|---|
| | 11. SPONSOR/MONITOR'S REPORT NUMBER(S) |

**12. DISTRIBUTION/AVAILABILITY STATEMENT**

Approved for public release; distribution unlimited.

**13. SUPPLEMENTARY NOTES**

**14. ABSTRACT**

This technical report presents a time-domain moving-target indication (MTI) processing formulation for detecting slow-moving personnel behind walls. We demonstrate the effectiveness of the MTI processing formulation using data collected by the U.S. Army Research Laboratory's (ARL) ultra-wideband (UWB) synchronous impulse reconstruction (SIRE) radar. The resulting data set is representative of multiple operational scenarios including personnel walking inside wood and cinderblock structures; personnel walking in linear and nonlinear trajectories; and multiple personnel walking within the same building structure. The results indicate that our time-domain MTI processing formulation can identify moving targets even when they move slowly along trajectories that are not favorable for classical, Doppler-based MTI.

**15. SUBJECT TERMS**

moving target indication, impulse radar, target tracking, change detection, clutter cancelation, clustering, CFAR

| 16. SECURITY CLASSIFICATION OF: | | | 17. LIMITATION OF ABSTRACT | 18. NUMBER OF PAGES | 19a. NAME OF RESPONSIBLE PERSON |
|---|---|---|---|---|---|
| a. REPORT | b. ABSTRACT | c. THIS PAGE | | | Anthony Martone |
| Unclassified | Unclassified | Unclassified | UU | 36 | 19b. TELEPHONE NUMBER (*Include area code*)<br>(301) 394-2531 |

## Contents

**List of Figures** **iv**

**1. Introduction** **1**

**2. MTI Time-Domain Phenomenology** **3**

2.1 Change Detection ....3

2.2 Constant False Alarm Rate (CFAR) Approach....5

2.3 Clustering Analysis ....9

2.4 Tracker....14

**3. Experiments** **15**

**4. Conclusions** **23**

**5. References** **25**

**List of Symbols, Abbreviations, and Acronyms** **27**

**Distribution List** **28**

## List of Figures

Figure 1. The SIRE radar. ..... 2

Figure 2. MTI processing formulation. ..... 2

Figure 3. Block diagram detailing steps involved in Image Formation and Change Detection steps of the processing chain of figure 2. ..... 3

Figure 4. Two SAR images of a target area with a moving target present; the location of the mover is unknown. ..... 4

Figure 5. Difference image generated by applying change detection to the SAR images in figure 4; the MT signature is clearly identifiable. ..... 5

Figure 6. Example CFAR window, made of an inner, guard, and outer window. ..... 6

Figure 7. Example of a CFAR window placed over the MT signature, where the inner window is overlaid on the MT signature and the outer window covers the background of the local area. The inner window contains pixels with higher energy compared with the pixels contained in the outer window. ..... 6

Figure 8. The difference image is input into the CFAR algorithm and the CFAR image is output. The red cluster in the CFAR image corresponds to a group of POIs. ..... 9

Figure 9. Example of a difference image and the resulting CFAR image. The CFAR image contains false MT signatures (i.e., false alarms). ..... 9

Figure 10. The CFAR image contains POIs. When the CFAR image is input into a clustering algorithm, two clusters are identified; the clusters and corresponding centroids are shown in the cluster image. ..... 10

Figure 11. The k-Means algorithm. ..... 11

Figure 12. k-Means algorithm iteration example: the red line indicates progression of the first mean vector and the black line indicates progression of the second mean vector. Multiple iterations are needed to minimize the error between the POIs and nearest mean vectors. ..... 12

Figure 13. CFAR images with POIs present. Through a visual inspection of the CFAR images, it would appear that two clusters are present. ..... 13

Figure 14. A plot of NMSOS errors for different values of N—a large gap exists between N=1 and N=2, thereby indicating the N=2 is the knee-point. ..... 14

Figure 15. A block diagram of the modified tracker algorithm. ..... 15

Figure 16. Building plan and geometry of Scenario 1: a man is walking inside of a cinderblock building. ..... 16

Figure 17. Cinderblock building images for Scenario 1. ..... 16

Figure 18. Imagery from the MTI output for Scenario 1 with circles indicate location of walking man. The front wall and “ghosts” on the back wall are both visible. ..... 17

Figure 19. Photos and frames for Scenario 2 that depict two men walking in opposite directions downrange from the radar. ..... 18

Figure 20. Photos and frames for Scenario 3 that depict two men walking in opposite directions cross-range from the radar. .....19

Figure 21. Photos and frames for Scenario 4 that depict one person moving in a circular pattern. .....20

Figure 22. Tracker output of the person walking in a circle; the black squares are the positions of the centroids, the red diamonds are the positions estimated by the tracker, and the red line is the path of the moving person as estimated by the tracker.....21

Figure 23. Photos and frames for Scenario 5: the man enters the room (Frames 1 and 2), sits down in the chair, fidgets a while (Frames 3 and 4), and then stands and exits the room (Frames 5 and 6). .....22

Figure 24. Tracker output of the person walking into a room, sitting in a chair, and leaving the room. The black squares are the positions of the centroids, the red diamonds are the positions estimated by the tracker, and the red line is the estimated path of the moving person output by the tracker.....23

INTENTIONALLY LEFT BLANK.

# 1. Introduction

Current and future forces operating in urban environments need the capability to detect slow-moving personnel behind walls. One approach to moving-target indication (MTI) of slow-moving personnel is a frequency-domain approach, i.e., Doppler processing (*1*). Doppler-processing techniques separate the moving target from background clutter by exploiting the Doppler shift in backscattered frequency that is caused by the velocity of the moving target. The challenge to the frequency-domain approach is the very small Doppler shift in backscattered frequency from slow-moving personnel. Therefore, we consider a time-domain approach, namely a change detection paradigm, which is inherently similar to clutter cancellation (*1, 2*).

In this report, we demonstrate the detection of slow-moving personnel behind walls using the U.S. Army Research Laboratory's (ARL) ground-based, synchronous impulse reconstruction (SIRE) radar system (*3*), which was designed to detect concealed targets (*4*). The SIRE radar is an impulse-based, ultra-wideband (UWB) imaging radar with a bandwidth covering 300 MHz to 3 GHz. The low frequencies make it possible to image inside buildings and detect slow-moving targets (*5*).

The SIRE radar employs a physical aperture of 16 receiver antennas. These antennas are equally spaced across a linear aperture that is approximately 2 m long. Two impulse transmitters are located at either end and slightly above the receive array, as illustrated in figure 1. The transmitters fire in an alternating sequence—the left transmitter followed by the right. Each transmitter launches a sequence of low-power pulses, and reflected energy is integrated within each receive channel to achieve an acceptable signal-to-noise ratio (SNR). The SIRE radar constructs a high-resolution (0.056 m) downrange profile through novel, ARL-developed signal-processing techniques (*6*). In addition to high downrange resolution obtained via the UWB SIRE waveform, the system also achieves enhanced cross-range resolution through coherent processing of the signals measured simultaneously by the 16 receivers. The downrange swath measured by the radar extends from approximately 10 to 35 m, and the amount of processing time required for downrange profile reconstruction results in a low effective sampling rate (approximately one-third of a second). Finally, we recall that the operational frequencies of the SIRE system (300 MHz to 3 GHz) are appropriate for sensing-through-the-wall (STTW) applications (*7*). Hence, we have leveraged the SIRE radar as part of an overall investigation of MTI phenomenology.

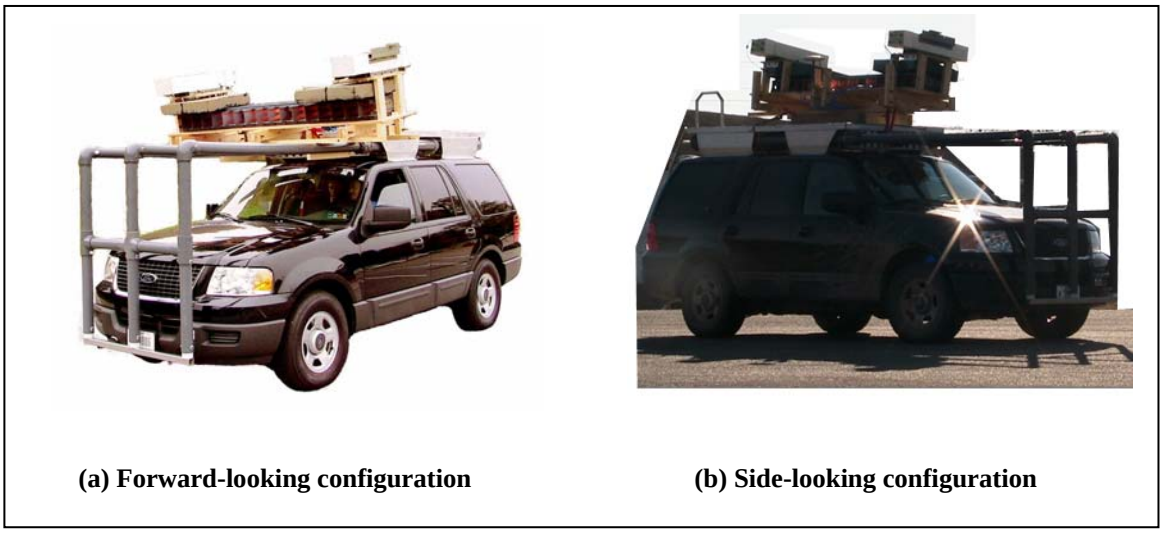

**(a) Forward-looking configuration** **(b) Side-looking configuration**

Figure 1. The SIRE radar.

We developed the MTI processing formulation shown in figure 2. The SIRE radar remains stationary and measures the energy reflected from an area under surveillance, or "target area." The 16 receive channels are processed using a time-domain back-projection technique developed for synthetic-aperture-radar (SAR) image formation (*8*). The SAR image, output of the first block in figure 2, contains several artifacts making it difficult to identify the moving target. Change detection is applied to the SAR images, thereby creating a set of difference images. Most of the artifacts due to stationary clutter are eliminated using change detection, and the moving target (MT) signature is revealed. Since some artifacts are still present in the difference images, additional processing is needed and implemented by an automatic target detection (ATD) algorithm. For example, the ATD algorithm reduces sidelobe artifacts and produces an ATD image that contains points of interest (POIs) corresponding to true and false MT signatures. One method to separate the false MT signatures from the true MT signatures is to implement a tracking algorithm. The number of POIs must first be reduced by identifying a centroid for each cluster of POIs. The centroids are input into the tracker and the tracker identifies a reasonable trajectory of the true moving target, thus allowing for the elimination of false MT signatures.

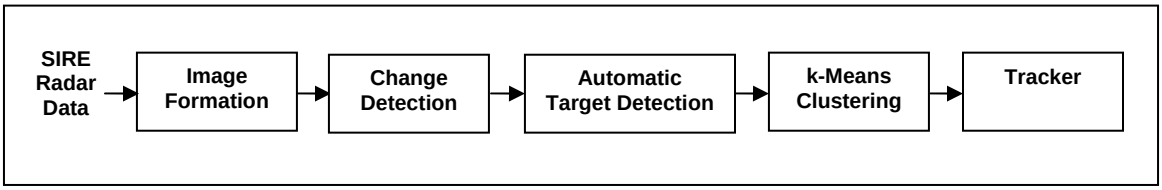


Figure 2. MTI processing formulation.

## 2. MTI Time-Domain Phenomenology

### 2.1 Change Detection

The first two blocks of the processing chain of figure 2 constitute the time-domain MTI processing required to create the MT signatures serving as input to the ATD algorithm. An additional block diagram detailing the implementation of this MTI processing is included in figure 3, and, as indicated, the MTI processing output flows directly into the ATD algorithm block of figure 2. In this section, we describe the entire procedure outlined in figure 3 in some detail.

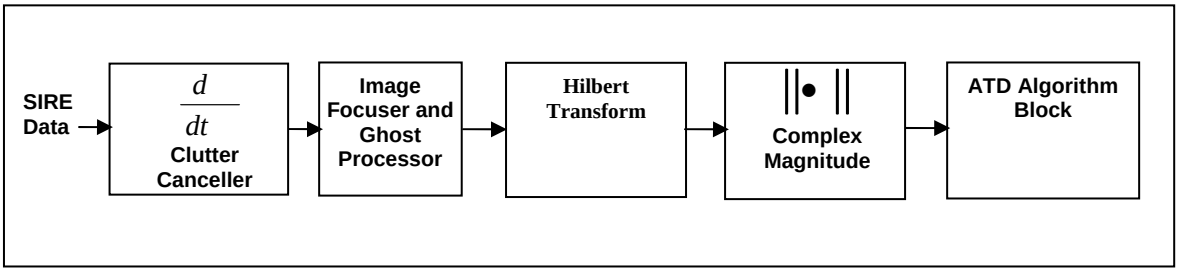


Figure 3. Block diagram detailing steps involved in Image Formation and Change Detection steps of the processing chain of figure 2.

We begin the MTI processing by buffering downrange profiles measured by each receive channel for a single pair of transmit pulses. Since the transmitters fire in sequence—the left transmitter followed by the right transmitter—we effectively buffer two downrange profiles from each receive channel, and the time required to assemble these profiles represents one data collection interval. After buffering the data from one collection interval, we then collect another pair of downrange profiles from each receive channel during the next data collection interval. Finally, we form the coherent difference between these newly collected profiles and the corresponding buffered profiles to obtain a new data set consisting of modified downrange profiles defined by

$$\dot{f}_{i,j,k}(r) = f_{i+1,j,k}(r) - f_{i,j,k}(r),\ i = 1,\ldots,N-1,\ j = 1,2,\ \text{and}\ k = 1,\ldots,16. \qquad (1)$$

Here $r$ represents the downrange index, $i$ represents the time index, $j$ represents the transmitter index, and $k$ represents the receiver index. Hence, we are forming a signal that monitors changes between the two sets of downrange profiles measured at time $i$ and time $i$+1 using transmitter $j$ and receiver $k$. This is why we refer to our model as a "change detection" (CD) paradigm. The difference signal, $\dot{f}_{i,j,k}(r)$ (corresponding to the derivative in time), is then input to an image formation routine, in our case a time-domain back-projection procedure, resulting in the output difference image,

$$I_{diff}(x,y) = \sum_{k=1}^{16} \sum_{j=1}^{2} \sum_{i=1}^{N-1} g(i,j,k)\, \dot{f}_{i,j,k}(r_{i,j,k}), \tag{2}$$

where $g(i,j,k)$ is a scaling function. To illustrate the effectiveness of the CD approach, consider the SAR images in figures 4a and 4b. The SAR images are focused on the same target area at different moments in time without forming the difference, and one person is moving within the target area. SAR Image 1, $I_1(x,y)$, was focused by our back-projection procedure using downrange profiles $\{f_{1,1,1}(r),\ldots f_{1,1,16}(r)\}$. SAR Image 2, $I_2(x,y)$, was focused by our back-projection procedure using downrange profiles $\{f_{2,1,1}(r),\ldots f_{2,1,16}(r)\}$. As is evident, the SAR images contain several artifacts making it difficult to identify the moving target. The moving target is located by applying change detection. The resulting difference image is shown in figure 5. It is clear from the difference image that most of the artifacts due to stationary clutter have been eliminated and the resulting MT signature is identified.

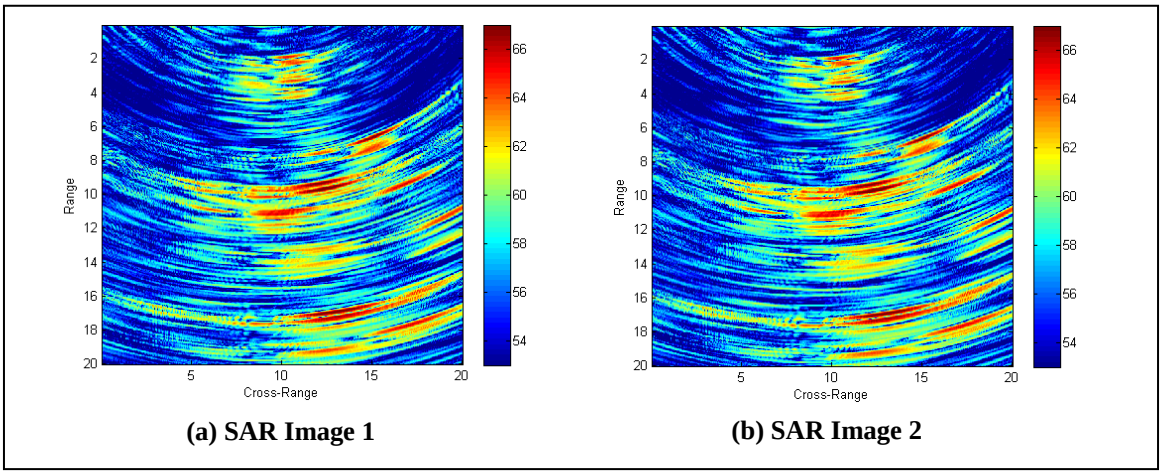


**(a) SAR Image 1** **(b) SAR Image 2**

Figure 4. Two SAR images of a target area with a moving target present; the location of the mover is unknown.

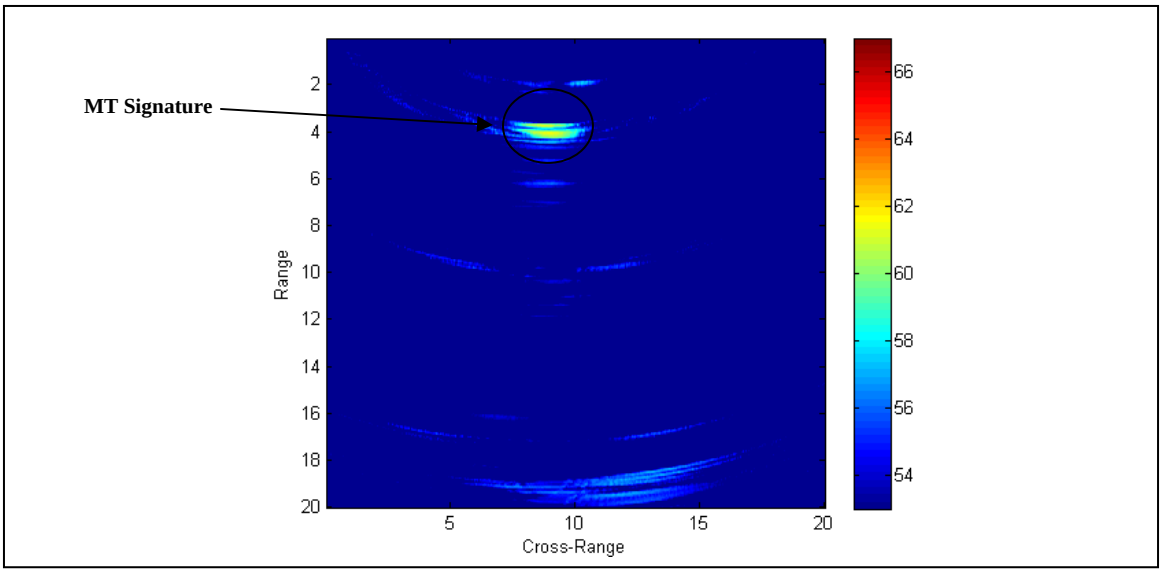


Figure 5. Difference image generated by applying change detection to the SAR images in figure 4; the MT signature is clearly identifiable.

## 2.2 Constant False Alarm Rate (CFAR) Approach

Interpretation of the resulting MT signature is still challenging after change detection. For example, change detection cannot automatically identify the MT signature located in the difference image and the MT signature can only be identified through visual inspection of a sequence of difference images. Therefore, it is not possible to implement additional signal processing techniques like classification using a single difference image. Another challenge with change detection is that sidelobe artifacts are produced in the difference image, which confuse the true moving target location.

A way to improve user interpretation of the resulting difference image is to apply the CFAR algorithm. CFAR is a well-established approach to eliminating potential false alarms. Typically, the algorithm performs a test of local contrast that is designed to achieve a constant false alarm rate (*9*). For a given difference image $\mathrm{I}_{diff}(x, y)$, a CFAR window is used to scan the difference image and test for the MT signature. An example of a CFAR window is shown in figure 6, where $I_X$ and $I_Y$ are the inner windows' cross-range and range dimensions, respectively; $G_X$ and $G_Y$ are the guard windows' cross-range and range dimensions; and $O_X$ and $O_Y$ are the outer windows' cross-range and range dimensions. The inner window dimensions are designed so that it is overlaid on the MT signature. When the inner window is overlaid on the MT signature, the outer window dimensions are designed to be superimposed on the local background. The guard window is used as a buffer between the inner and outer windows and ensures that large pixel values due to target sidelobes are not captured by the outer window. For example, consider the window that is placed in the difference image shown in figure 7. As is illustrated in the figure, the inner window is overlaid on the MT signature pixels and the outer window is overlaid on the local background pixels.

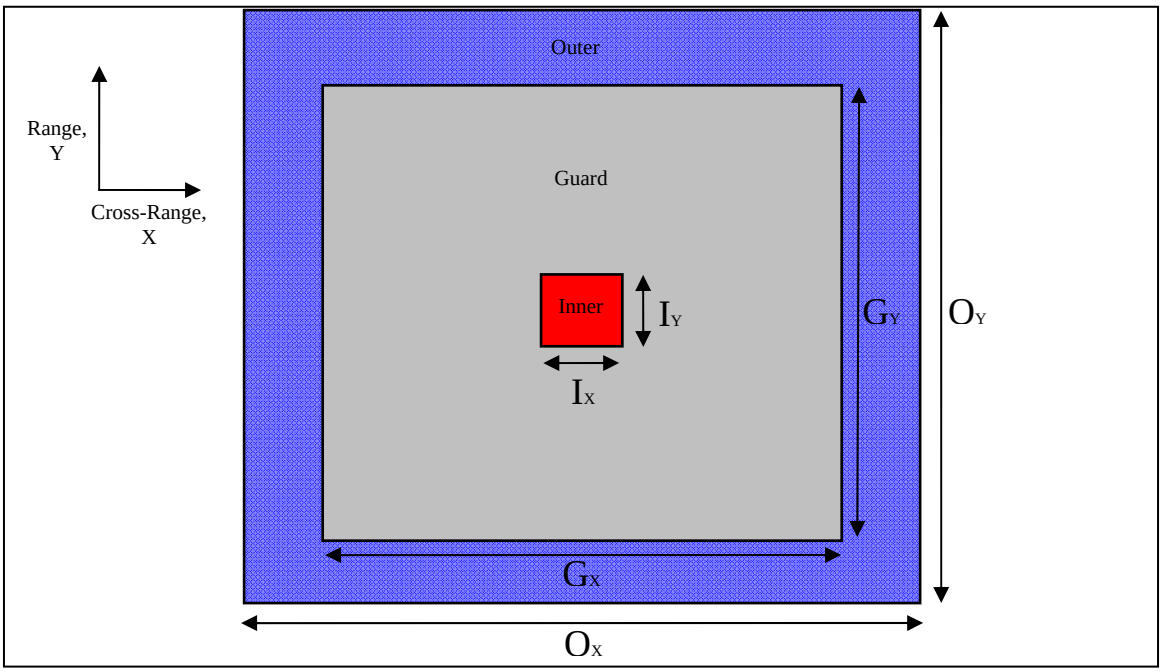


Figure 6. Example CFAR window, made of an inner, guard, and outer window.

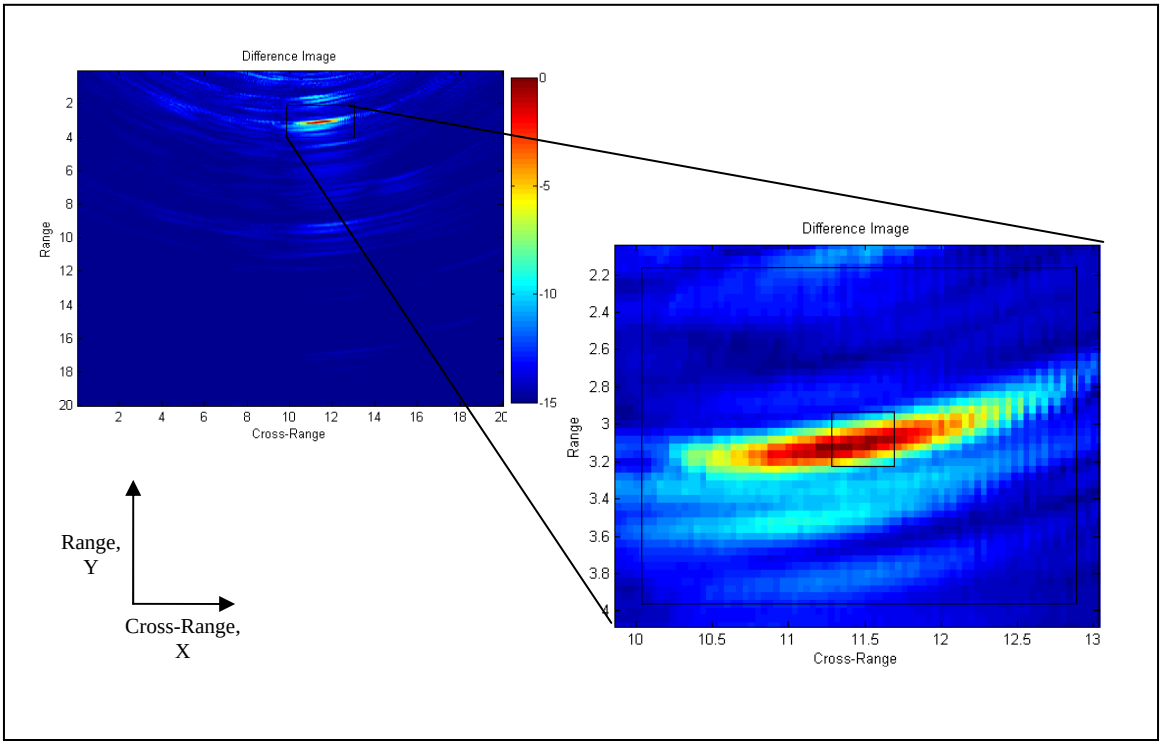


Figure 7. Example of a CFAR window placed over the MT signature, where the inner window is overlaid on the MT signature and the outer window covers the background of the local area. The inner window contains pixels with higher energy compared with the pixels contained in the outer window.

Based on our observations and analysis of the MT signatures, we have chosen the following dimensions for the CFAR window: $I_X = 7$, $I_Y = 9$, $G_X = 23$, $G_Y = 25$, $O_X = 27$, $O_Y = 29$. It is of interest to note that the dimensions of the inner window constitute a small rectangular shape, which is different from the elliptical patterns of the MT signatures. The rectangular shape is chosen since it is small enough to fit over the MT signatures. The small rectangular window is used as an alternative to an elliptical window since the size and shape of the pattern of the moving target changes depending on the range and cross-range of the mover's position.

The CFAR window is placed in the difference image of size $(500,500)$ and moved pixel by pixel over the entire difference image. Let the center of the CFAR window be positioned at coordinates $(X,Y)$ in the difference image, where $X \in \{\lceil O_X / 2 \rceil,...(500 - \lfloor O_X / 2 \rfloor)\}$ and $Y \in \{\lceil O_Y / 2 \rceil,...(500 - \lfloor O_Y / 2 \rfloor)\}$. The notation $\lfloor x \rfloor$ denotes the largest integer less than *x* for $x > 0$ (i.e., floor), and $\lceil x \rceil$ denotes the smallest integer greater than x for $x > 0$ (i.e., ceiling). The CFAR algorithm indicates an MT signature if the sum of the energy in the inner window is larger than the sum of the energy in the outer window. This is shown in figure 7, where the energy of the pixels in the inner window is larger then the energy of the pixels in the outer window. The inner window to outer window energy ratio is defined as

$$R = \frac{\mu_i}{\mu_o}, \tag{3}$$

where

$$\mu_i = \sum_k \sum_l [\Phi(P_{(l,k)})]^2 \tag{4}$$

is the sum of the energy in the inner window, $k = [Y - \lfloor I_Y / 2 \rfloor,...Y + \lfloor I_Y / 2 \rfloor]$, $l = [X - \lfloor I_X / 2 \rfloor,...X + \lfloor I_X / 2 \rfloor]$, and $P_{(l,k)}$ is the magnitude of the pixel at position $(l,k)$. Define

$$\Phi(P_{(l,k)}) = \begin{cases} P_{(l,k)}, & P_{(l,k)} > \eta \\ \eta, & P_{(l,k)} \le \eta \end{cases}, \tag{5}$$

where $\eta = \max(\mathrm{I}_{diff}(x,y))/2$ and $\max(\mathrm{I}_{diff}(x,y))$ is the maximum pixel magnitude in the difference image. The function $\Phi(P_{(l,k)})$ is used to adjust the image background and require that the magnitude of each pixel is above the threshold defined by $\eta$, which is done to prevent errors due to division by very small numbers. Division by very small numbers artificially inflates the ratio defined by equation 3 and causes false positives. The threshold $\eta$ was chosen based on the observations of the sidelobes corresponding to the MT signature, which are typically less than $\max(\mathrm{I}_{diff}(x,y))/2$ in magnitude. This choice of $\eta$ eliminates the sidelobes by blending them into the background of the difference image.

The sum of the energy in the outer window is defined as

$$\mu_o = E_W - E_{I+G}, \tag{6}$$

where

$$E_W = \sum_m \sum_n [\Phi(P_{(n,m)})]^2 \tag{7}$$

is the sum of the energy in the entire CFAR window, $m = [Y - \lfloor O_Y / 2 \rfloor, ... Y + \lfloor O_Y / 2 \rfloor]$, $n = [X - \lfloor O_X / 2 \rfloor, ... X + \lfloor O_X / 2 \rfloor]$, and define

$$E_{I+G} = \sum_q \sum_r [\Phi(P_{(r,q)})]^2 \tag{8}$$

as the sum of the energy in the guard and inner windows, where $q = [Y - \lfloor G_Y / 2 \rfloor, ... Y + \lfloor G_Y / 2 \rfloor]$ and $r = [X - \lfloor G_X / 2 \rfloor, ... X + \lfloor G_X / 2 \rfloor]$. Define a CFAR test as

$$\Psi = \begin{cases} 1 & R > 2 \\ 0 & else \end{cases}, \tag{9}$$

which requires that the sum of the energy in the inner window is more than twice the sum of the energy in the outer window. If $\Psi = 1$, then the center pixel (at coordinates $(X, Y)$) is a POI corresponding to an assumed moving target. The CFAR window scans the entire difference image and a list of POIs are identified. For example, consider the difference image and CFAR image of figure 8. The difference image is input into the CFAR algorithm and the CFAR image is output. The red cluster in the CFAR image corresponds to a group of POIs. This example illustrates that the CFAR algorithm identifies the MT signature and eliminates the sidelobe artifacts present in the difference image.

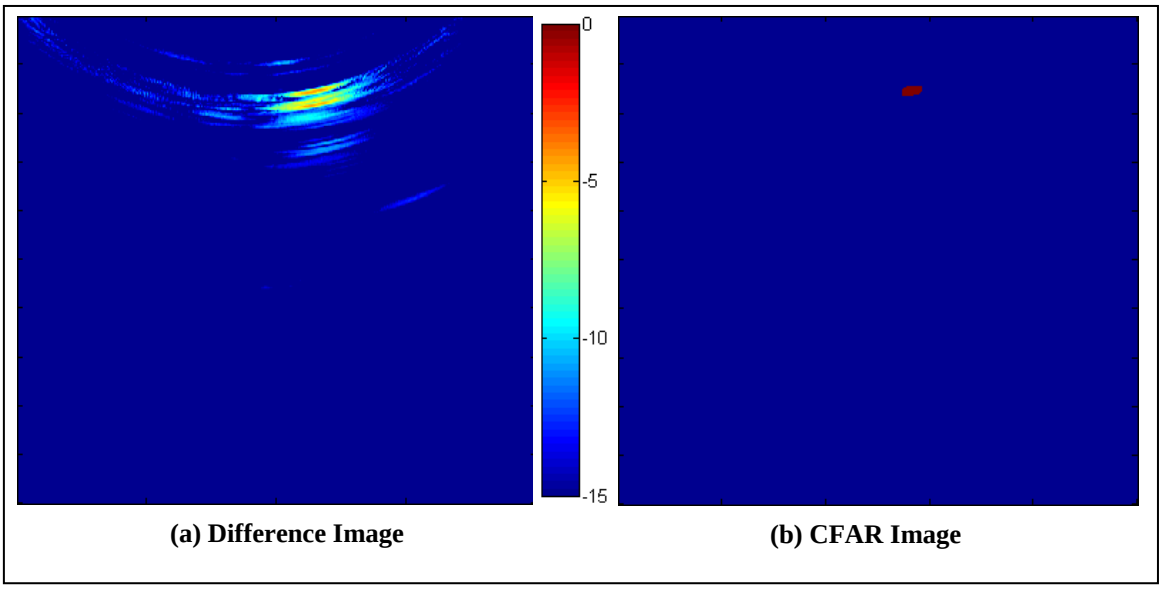


Figure 8. The difference image is input into the CFAR algorithm and the CFAR image is output. The red cluster in the CFAR image corresponds to a group of POIs.

## 2.3 Clustering Analysis

The POIs provide us with a list of possible moving target locations; however, some POIs may correspond to false alarms. For example, consider the difference image and CFAR image shown in figure 9. As illustrated, the difference image contains true MT signatures and false MT signatures, i.e., false alarms. As is shown in the CFAR image, the CFAR algorithm does not eliminate all false alarms. One possible way to eliminate the false alarms is to input the POIs into a tracking algorithm. The tracking algorithm examines the positions of the POIs over a period of time and identifies a reasonable trajectory. Any POI not part of the trajectory is considered as a false alarm.

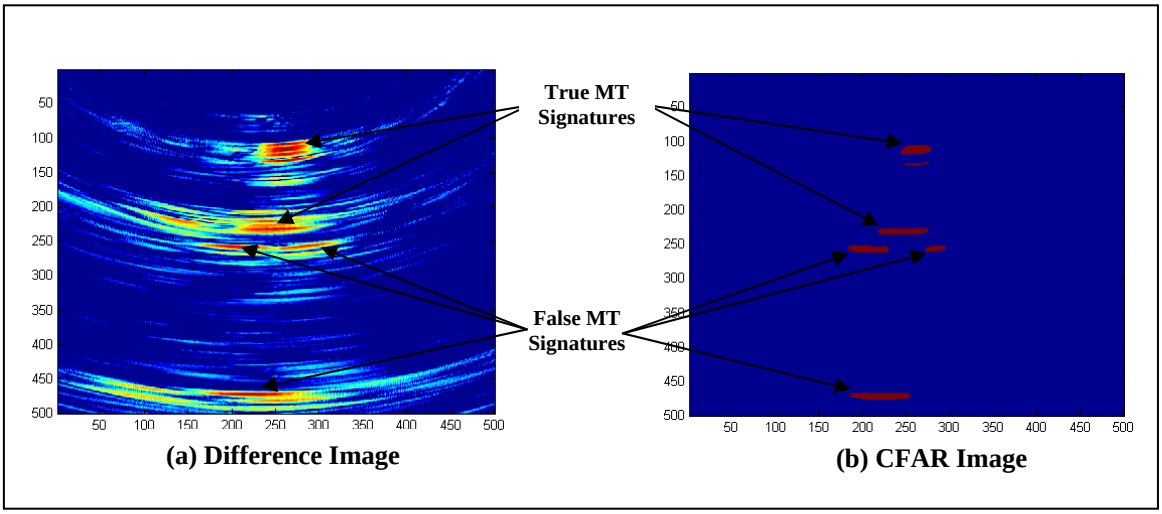


Figure 9. Example of a difference image and the resulting CFAR image. The CFAR image contains false MT signatures (i.e., false alarms).

Before the POIs are input into a tracking algorithm, the number of POIs must be reduced. This motivates the need to refine the number of POIs by using a clustering algorithm to identify centroids for adjacent POIs. For example, consider the CFAR image shown in figure 10. The CFAR image (figure 10a) contains the POIs. When the CFAR image is input into a clustering algorithm, two clusters are identified. The clusters and corresponding centroids are shown in the cluster image (figure 10b). It should be noted that the clusters identified by the clustering algorithm are not unique and it is possible that the centroid locations differ for different iterations of the clustering algorithm.

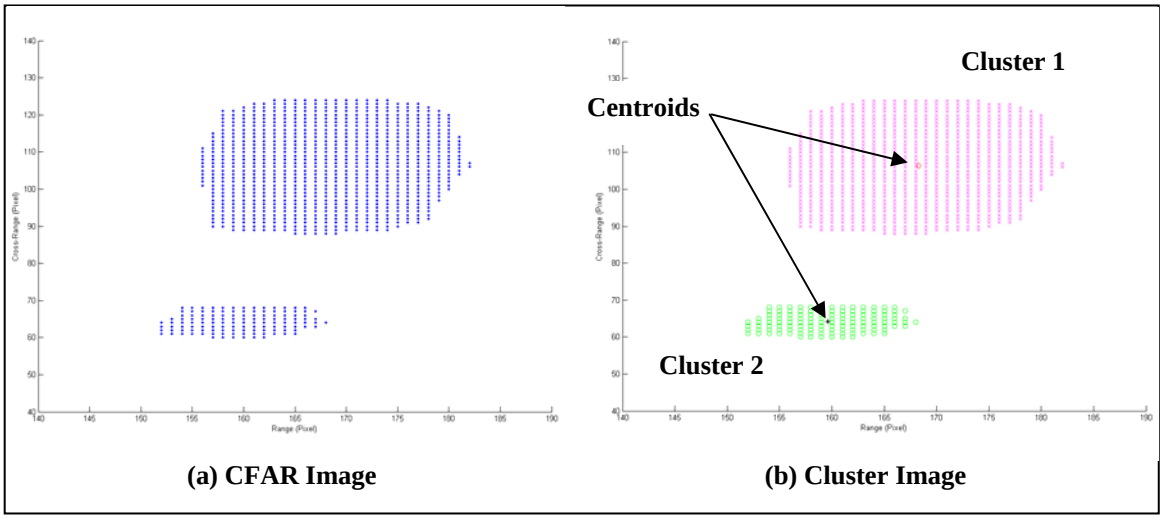


Figure 10. The CFAR image contains POIs. When the CFAR image is input into a clustering algorithm, two clusters are identified; the clusters and corresponding centroids are shown in the cluster image.

The clustering routine used by the MTI processing formulation of figure 2 is the well-known k-Means algorithm (*10*, *11*). The k-Means algorithm identifies the centroids of the POIs by an iterative procedure. This iterative procedure minimizes the square-error between centroid estimates and their corresponding POIs. A block diagram of the k-Means algorithm is shown in figure 11.

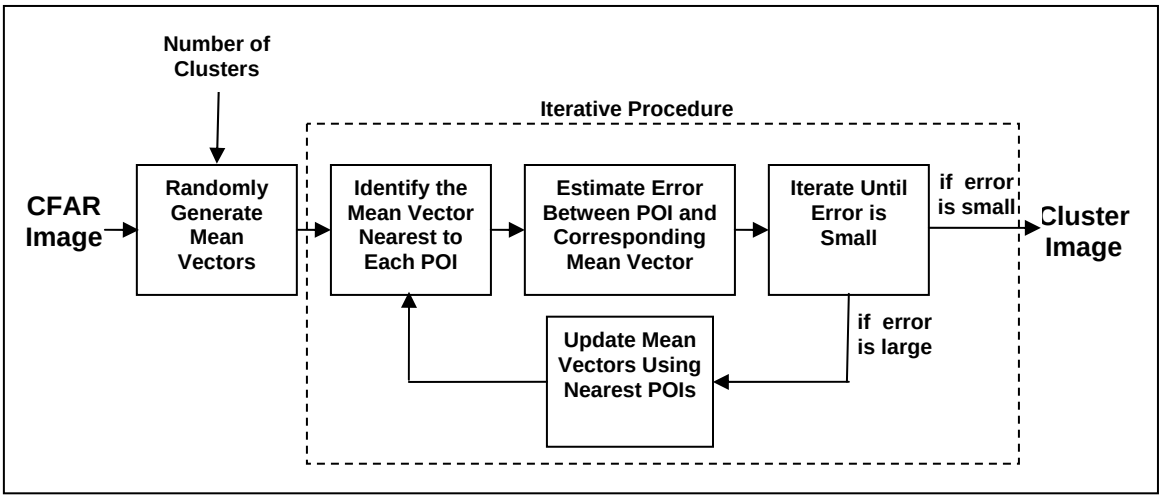


Figure 11. The k-Means algorithm.

The input CFAR image contains a set of $M$ POI vectors defined as

$$\{\rho_1,...\rho_M\}, \tag{10}$$

where $\rho_i = [\hat{\rho}_{(i,X)} \quad \hat{\rho}_{(i,Y)}]$ is the $i^{th}$ POI vector, $\hat{\rho}_{(i,X)}$ is the cross-range component of $\rho_i$, and $\hat{\rho}_{(i,Y)}$ is the range component of $\rho_i$. The k-Means algorithm requires that the number of clusters, $N$, is known a priori. The k-Means algorithm begins by randomly generating $N$ mean vectors defined as

$$\{\mu_1,...\mu_N\}, \tag{11}$$

where $\mu_j = [\hat{\mu}_{(j,X)} \quad \hat{\mu}_{(j,Y)}]$ is the $j^{th}$ mean vector, $\hat{\mu}_{(j,X)}$ is the cross-range component of $\mu_j$, and $\hat{\mu}_{(j,Y)}$ is the range component of $\mu_j$. The mean vectors are considered as centroid estimates. The next step of the algorithm determines the mean vector nearest to each POI using the Euclidean distance measure:

$$D_{(i,j)} = \| \mu_j - \rho_i \|^2. \tag{12}$$

Next define the set $S_j$ of size $m_j$ to be the POIs closest to $\mu_j$. Estimate the error between the mean and nearest POIs using the sum of squares (SOS) error criteria (*12*):

$$J_k = \sum_{j=1}^{N} \sum_{\rho_i \in S_j} \| \rho_i - \mu_j \|^2, \tag{13}$$

where $J_k$ is the error for the $k^{th}$ iteration of the k-Means algorithm. This SOS error criterion is a measure of variance between the POI vectors and the nearest mean vectors and must be minimized. The following equation is used to determine if $J_k$ is minimized:

$$| J_k - J_{k-1} | < \varepsilon , \tag{14}$$

where $J_{k-1}$ is the error for the (k–1) iteration, and $\varepsilon$ is a threshold value. If the condition defined by equation 14 is satisfied, then the SOS error is minimized, thereby indicating the final centroid estimates represented by the mean vectors. If the condition defined by equation 14 is not satisfied, then an additional iteration is required and each mean vector is updated using its nearest POI:

$$\mu_j = \frac{1}{m_j} \sum_{\rho_i \in S_j} \rho_i \ . \tag{15}$$

For example, consider the CFAR image in figure 12. For this example, two mean vectors were randomly generated and indicated by the red diamond and black star. As the k-Means algorithm iterates, several centroids are estimated. Each newly generated estimate corresponds to a smaller SOS error.

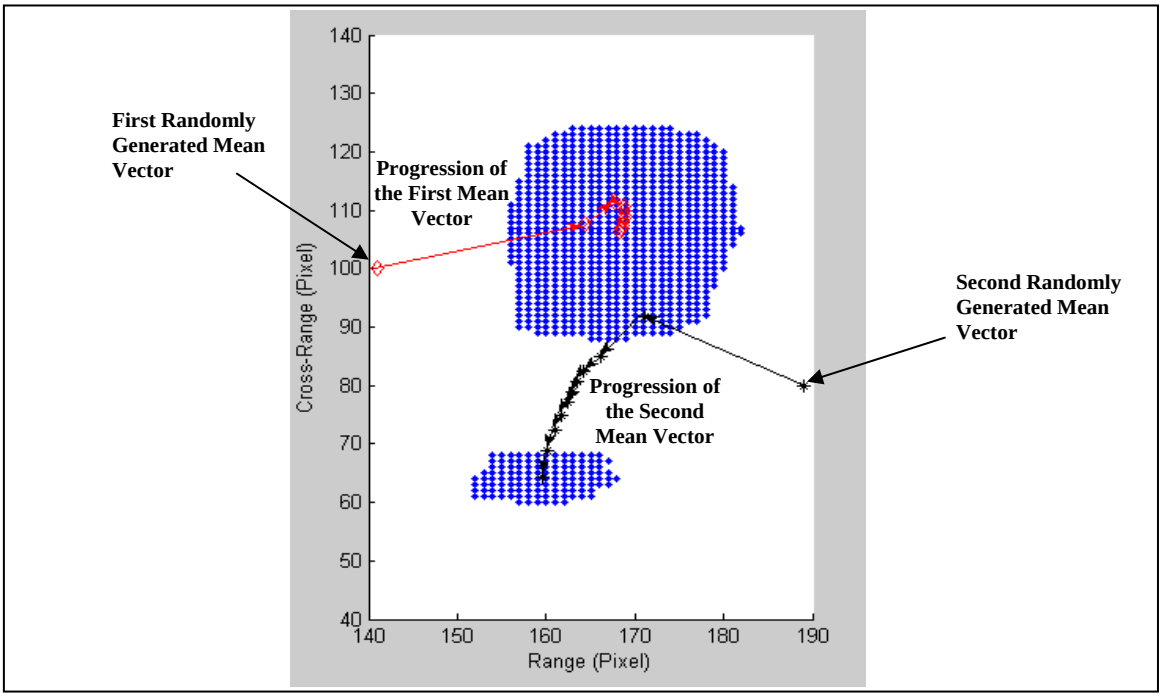


Figure 12. k-Means algorithm iteration example: the red line indicates progression of the first mean vector and the black line indicates progression of the second mean vector. Multiple iterations are needed to minimize the error between the POIs and nearest mean vectors.

A limitation of the k-Means algorithm is that the number of clusters $N$ must be known a priori. One approach to automatically determine the most reasonable number of clusters is to iterate the k-Means algorithm for many different cluster number choices. This will produce a set of minimized SOS errors $\hat{J} = \{\hat{J}_1, \hat{J}_2, ...\hat{J}_C\}$, where $\hat{J}_i$ is the *i*th minimized SOS error, and $i = 1, 2, \ldots, C$ denotes the number of clusters (i.e., $N$). We normalize $\hat{J}$ by $\max(\hat{J})$ to obtain $\bar{J} = \{\bar{J}_1, \bar{J}_2, ...\bar{J}_C\} = \hat{J} / \max(\hat{J})$, where $\bar{J}_i$ is the $i^{th}$ normalized minimized SOS error (NMSOS). A heuristic used to identify the proper value of $N$ plots $\{\bar{J}_1, \bar{J}_2, ...\bar{J}_C\}$ and searches for a large drop in NMSOS error, i.e., the "knee-point" (*13*, *14*). For example, consider the CFAR images shown in figure 13. By visual inspection it would appear that two clusters are present in the CFAR images. The NMSOS errors for each image of figure 13 are plotted in figure 14. As is shown in figure 14, a large gap exists between $N = 1$ and $N = 2$, thereby indicating that $N = 2$ is the knee-point.

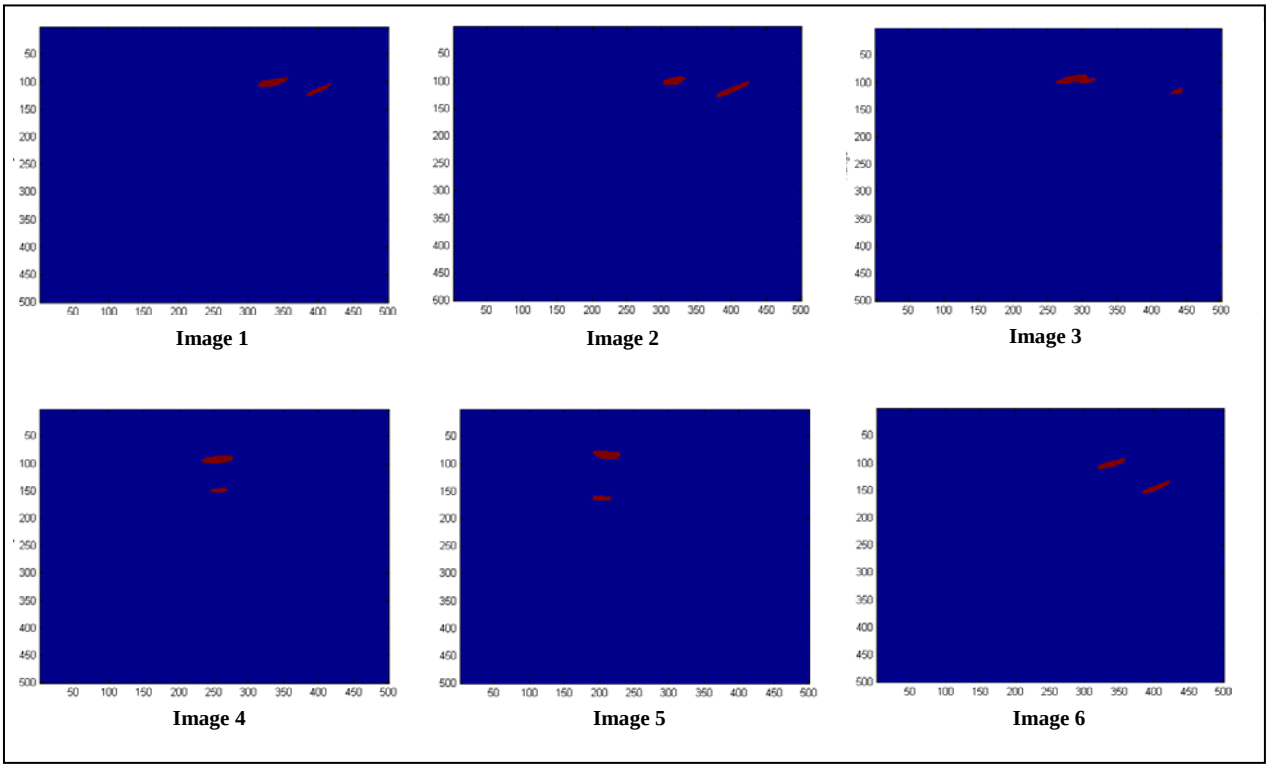


Figure 13. CFAR images with POIs present. Through a visual inspection of the CFAR images, it would appear that two clusters are present.

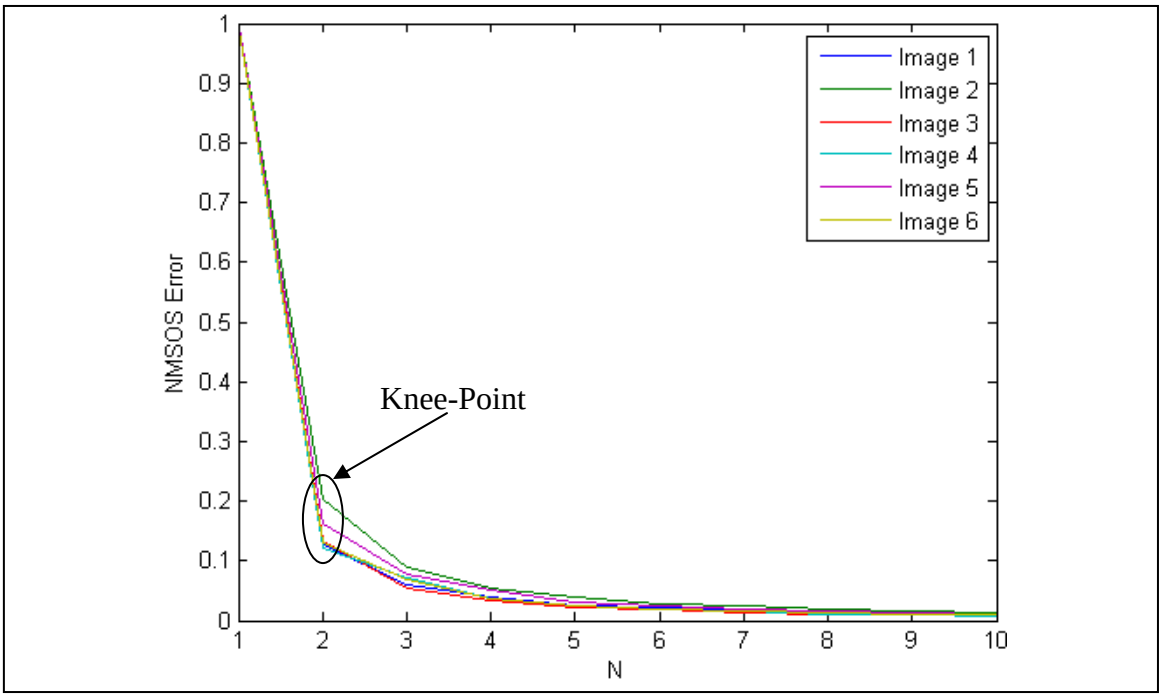


Figure 14. A plot of NMSOS errors for different values of N—a large gap exists between N=1 and N=2, thereby indicating the N=2 is the knee-point.

## 2.4 Tracker

The tracker algorithm is intended to reduce the number of false alarms and segregate targets from both clutter and one another as they move inside a building. The tracker implemented here is a modified version of an algorithm designed by Lincoln Laboratory for the purpose of tracking vehicles detected by an airborne radar platform (*15*). Since the amount of information received from the SIRE radar is not as comprehensive as the data received from the airborne platform, and since the slow motion of people can be more erratic than the motion of vehicles, it was necessary to substantially modify the tracker.

A block diagram of the modified tracker algorithm is shown in figure 15. The centroids generated by the clustering algorithm serve as inputs to the tracker; so it is possible to have multiple tracker inputs even when a single moving target is present. These centroids may indicate the true position of a moving target or false alarms. The tracker estimates the correlation between each centroid and the existing tracks and then associates the existing tracks with the most highly correlated (i.e., most reasonable) centroid. Non-assigned centroids are used to initiate new tracks and outdated tracks are deleted. A Kalman filter determines the present track position and predicts the next measurement.

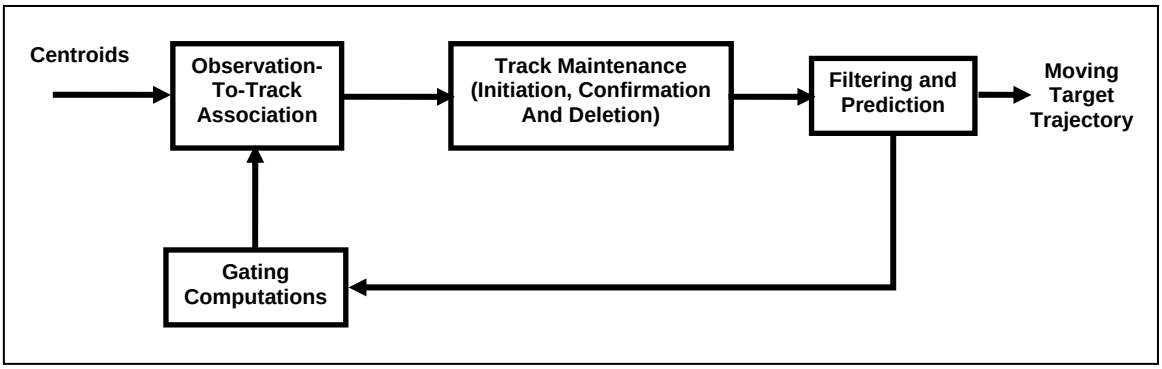


Figure 15. A block diagram of the modified tracker algorithm.

## 3. Experiments

The data for the experiments were collected during two separate field tests. The experiment for the first field test is referred to as Scenario 1 and was conducted in fiscal year (FY)07. Scenario 1 consisted of a single man walking in a room along a slight diagonal trajectory towards the radar, as illustrated in figure 16. The room was made of cinderblock walls with steel structural supports and a metal corrugated roof, supported by metal beams covered the single-story structure, as shown in figure 17. The building structure is rich in multi-path, as is inferred from the imagery in figure 17 (discussed later). The wide and relatively dark horizontal and vertical “stripes” evident in the wall (figure 17b) are composed of steel-reinforced concrete, and the metal frame can be seen at the top of each doorway. Hence, the structure represents a very difficult and challenging environment for detecting interior personnel due to the presence of thick lossy walls with numerous metallic supports in the walls and ceilings. Windows and doors provided an unobstructed view of the man at certain bearing angles, but most of his positions were obscured, at least to some extent, by the wall.

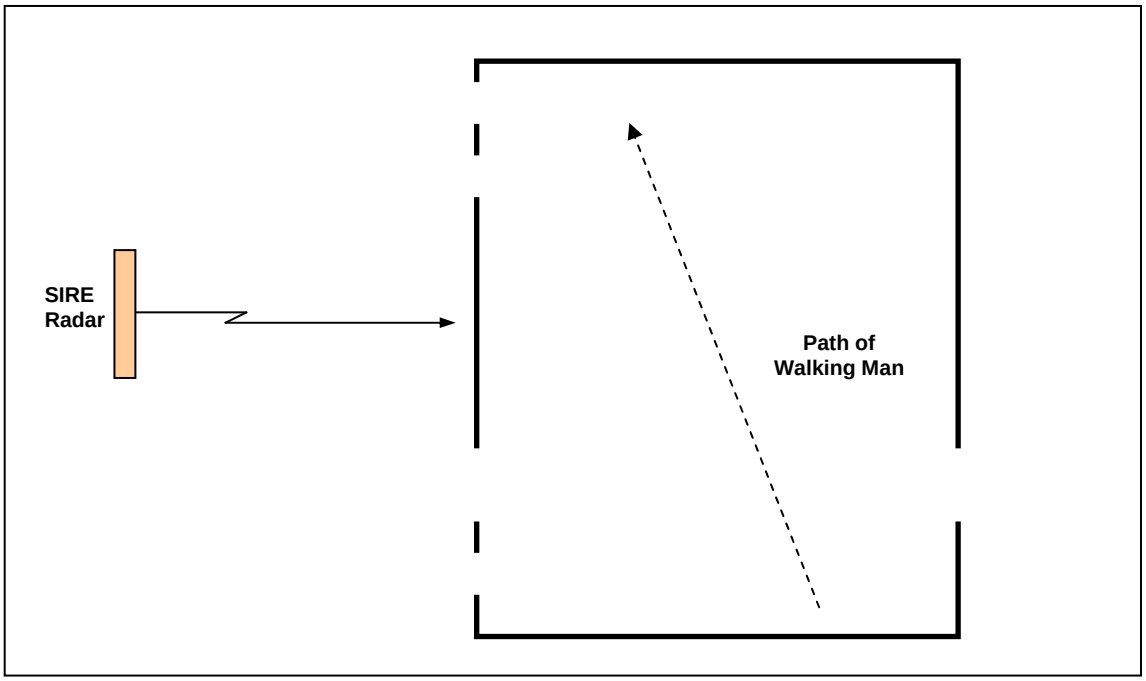


Figure 16. Building plan and geometry of Scenario 1: a man is walking inside of a cinderblock building.

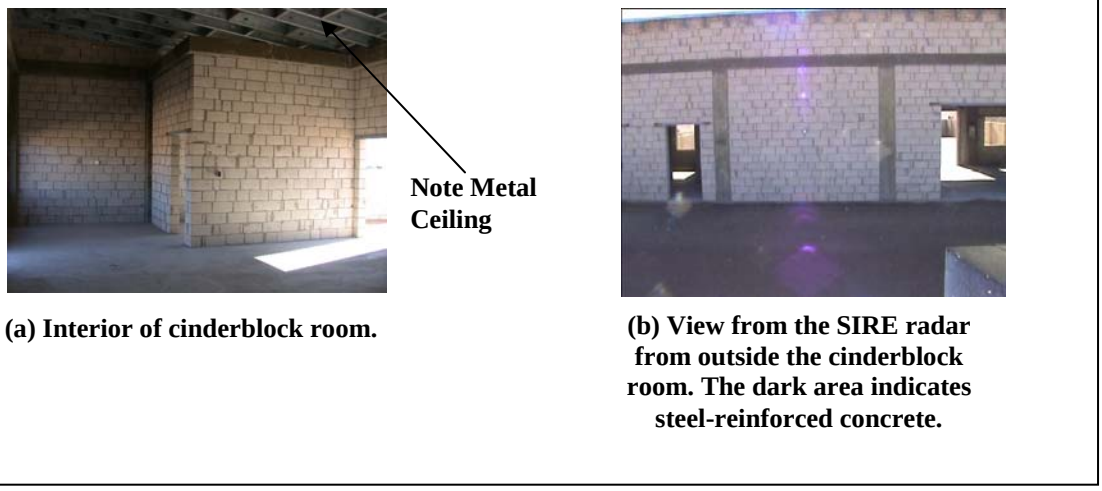


**(a) Interior of cinderblock room.**

**(b) View from the SIRE radar from outside the cinderblock room. The dark area indicates steel-reinforced concrete.**

Figure 17. Cinderblock building images for Scenario 1.

We implemented change detection for the data collected in Scenario 1. We are able to track the target manually by considering the difference images shown in figure 18. Note that for this data we have not implemented any additional processing (ATR, clustering, or tracking). The front wall of the building is evident as a bright ring in the near ranges. As is evident in the figure, certain artifacts ("ghosts") appear along the back wall. Modeling calculations indicated that such a phenomenon is to be anticipated due to the radar shadow cast on the back wall by the walking man.

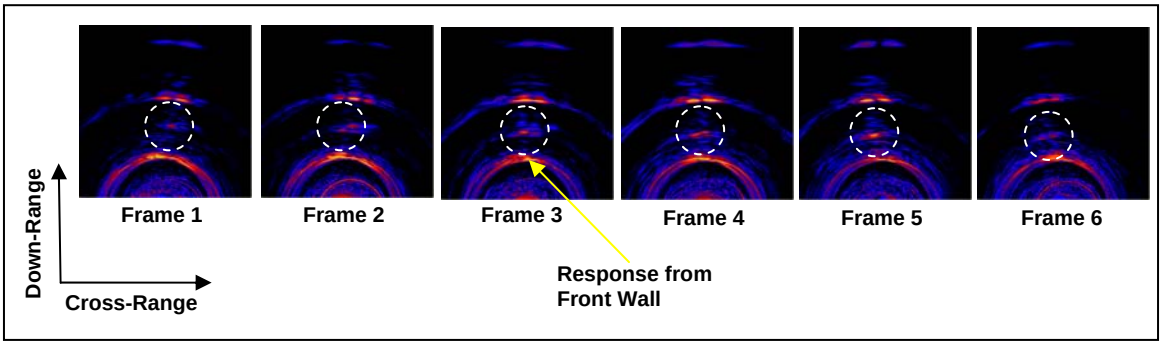


Figure 18. Imagery from the MTI output for Scenario 1 with circles indicate location of walking man. The front wall and "ghosts" on the back wall are both visible.

Data for Scenarios 2–5 were collected during the second field test. It included a building constructed of wood, with a stucco-like exterior finish applied to provide the appearance of brick. The scenarios generally played out within this building, and they included either multiple movers following linear trajectories or a single mover following a nonlinear trajectory. We implemented change detection, ATR, and clustering algorithms on the data for Scenarios 2–3 and implemented change detection, ATR, clustering, and tracking algorithms on the data for Scenarios 4–5.

Scenario 2 in figure 19 depicts two men walking in opposite directions (one toward the radar and the other away from it). Frame 1 indicates two movers present in the target area. Mover 1 is at the far downrange position (top of frame) and mover 2 is at the near downrange position (bottom of frame). The remaining frames show that the MT patterns move toward one another, cross, and move away from one another. We note that a favorable value for the number of centroids (one of the parameters required for the k-Means algorithm) was selected a priori for this, and the remaining, scenarios. Ultimately we are hoping to determine this value automatically. The process for estimating the optimal number of centroids is still one of our open topics of investigation. In this scenario we observe the presence of potential false alarms in some of these frames (e.g., Frame 3). It is also possible, as shown in Frame 3, that the CFAR algorithm eliminates (incorrectly) the MT signature of the first moving target. The downrange position of the moving target affects the size and shape of the MT signature as shown in the majority of the frames (some MT signatures are "long" and some are "short"). As mentioned in section 2.2, this inconsistency led us to choose a small rectangular inner window for the CFAR algorithm.

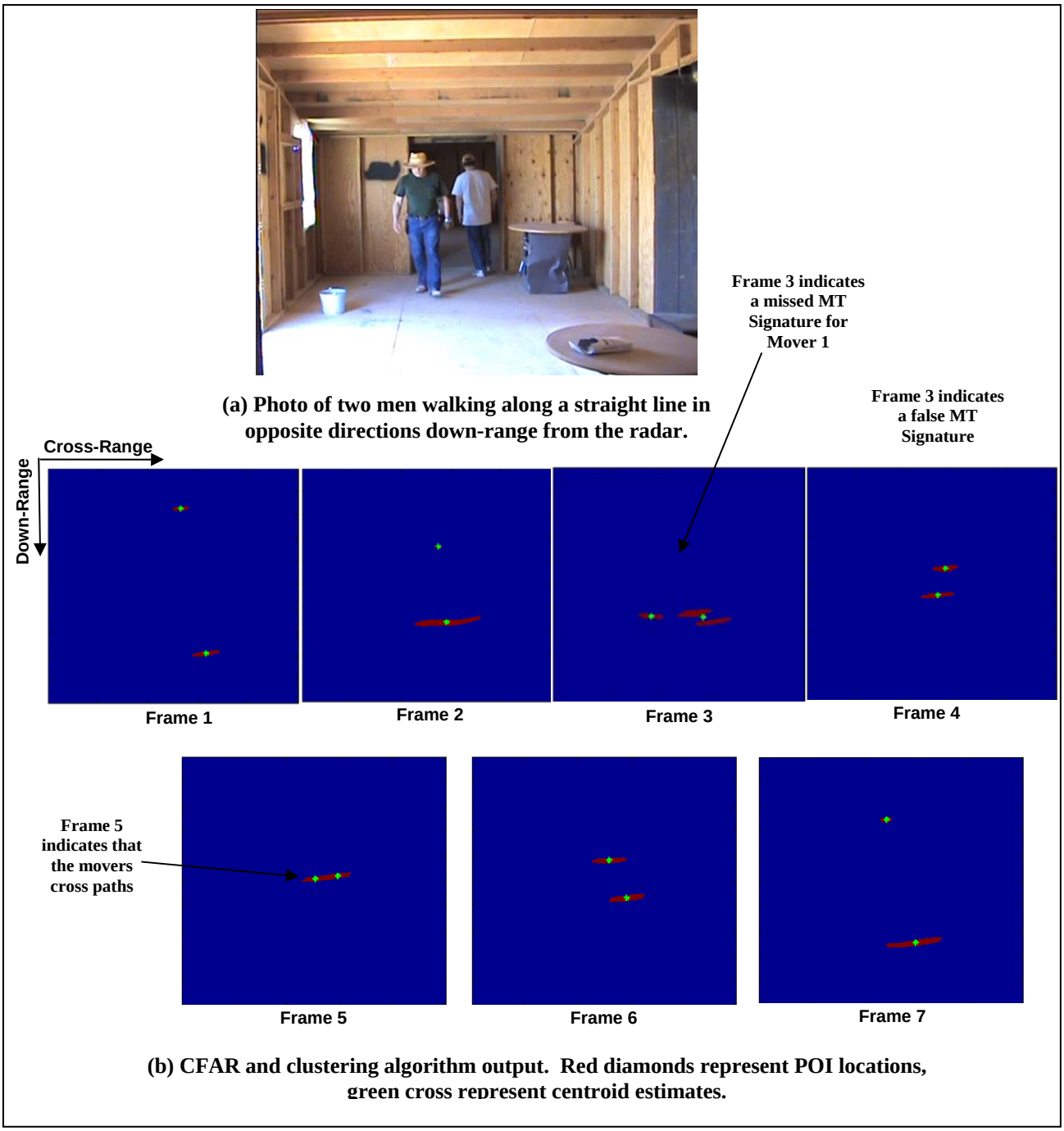


Figure 19. Photos and frames for Scenario 2 that depict two men walking in opposite directions downrange from the radar.

Scenario 3 is similar to Scenario 2 (two people walking) except that the target motion is perpendicular to the radar's line-of-sight, as shown in figure 20. Frame 1 depicts 2 movers present in the target area. Mover 1 is at the center of the frame and Mover 2 is at the right of the frame. Note that false alarms are generated by the CFAR algorithm. Since we knew the number of clusters a priori, the clustering algorithm identified the centroid of Mover 1 and eliminated the

false alarms generated by the CFAR algorithm. The remaining frames illustrate that the MT patterns move toward each other, cross, and move away from each other. Once again the ATD algorithm was able to localize the movers and assign several POIs to them, although we did again observe some potential false alarms in Frames 1 and 2 and missing MT signatures in Frames 2 and 4.

**(a) Photo of two men walking along a straight line in opposite directions cross-range to the radar.**




**(b) CFAR and clustering algorithm output. Red diamonds represent POI locations, green cross represent centroid estimates.**

Figure 20. Photos and frames for Scenario 3 that depict two men walking in opposite directions cross-range from the radar.

Scenario 4 is of a single man walking clockwise in a circular path as shown in figure 21a. The frames in figure 21b depict how the POI and centroid locations evolve as the ATD algorithm processed the input data stream. These frames indicate that the motion of the person walking in a circular pattern is identifiable by the centroids. Frame 1 is of the person moving away from the radar ("2 o'clock" position on the circular trajectory), frame 2 is of the person moving toward the radar ("9 o'clock" position on the circular trajectory), and frame 3 is of the person moving in cross-range relative to the radar ("12 o'clock" position on the circular trajectory). Figure 22 shows the track for a single target walking in a circular path. As is illustrated, three false alarms were generated by the CFAR algorithm. Due to the proximity of these false alarms in both space and time, the tracker has initiated an incorrect track. The detections of the real target have enough continuity to allow the tracking of this target during the entire period of motion.

**(a) Photo of person walking in a circular pattern.**

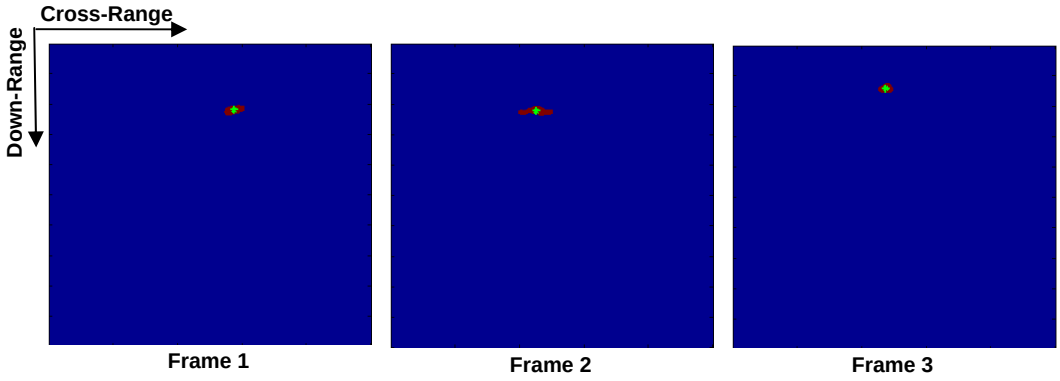


**(b) CFAR and clustering algorithm output. Red diamonds represent POI locations, green cross represents centroid estimates.**

Figure 21. Photos and frames for Scenario 4 that depict one person moving in a circular pattern.

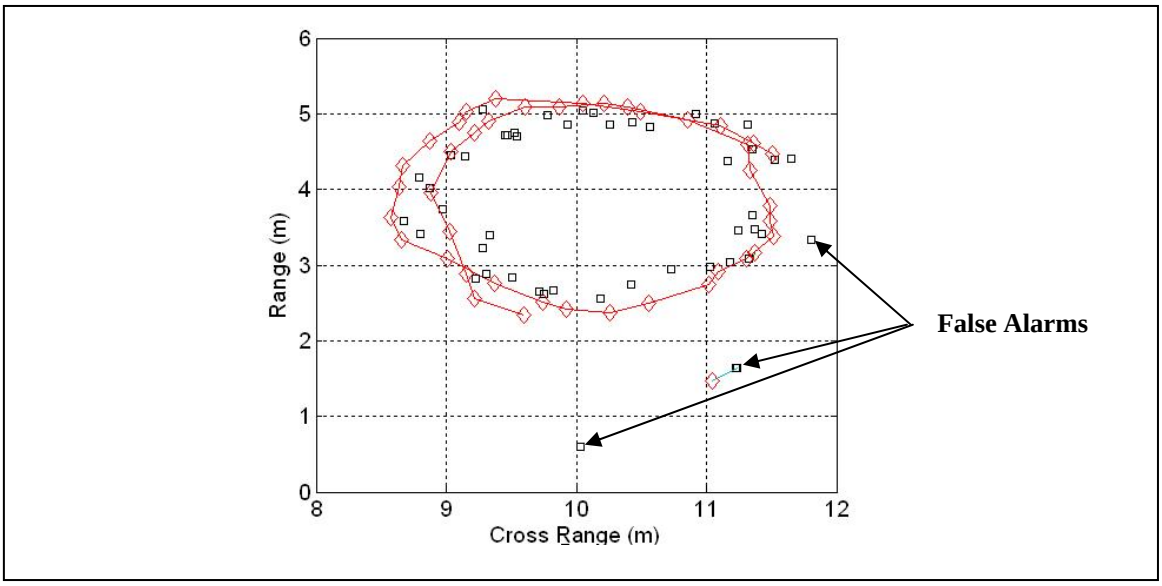


Figure 22. Tracker output of the person walking in a circle; the black squares are the positions of the centroids, the red diamonds are the positions estimated by the tracker, and the red line is the path of the moving person as estimated by the tracker.

Scenario 5, shown in figure 23, is substantially different than the previous scenarios in that it examined what would happen if a man entered a room, sat down in a chair, fidgeted while sitting, and then stood up and exited the room. Frames 1 and 2 depict the person moving toward the radar. Frames 3 and 4 depict the person sitting in the chair. Frames 5 and 6 depict the person moving away from the radar. False alarms are indicted in Frames 3 and 4. However, the MTI algorithms are able to identify and locate the person even when he is sitting. As illustrated in figure 24, the tracker followed the target when he entered the room, sat in the chair, and left the room. Several false alarms generated by the CFAR algorithm were disregarded by the tracker. The tracker lost the track of the moving person twice, but in each case was able to recover it due to the confined space in which the movement occurred.

**(b) Photo of a man sitting in a chair downrange from the radar.**

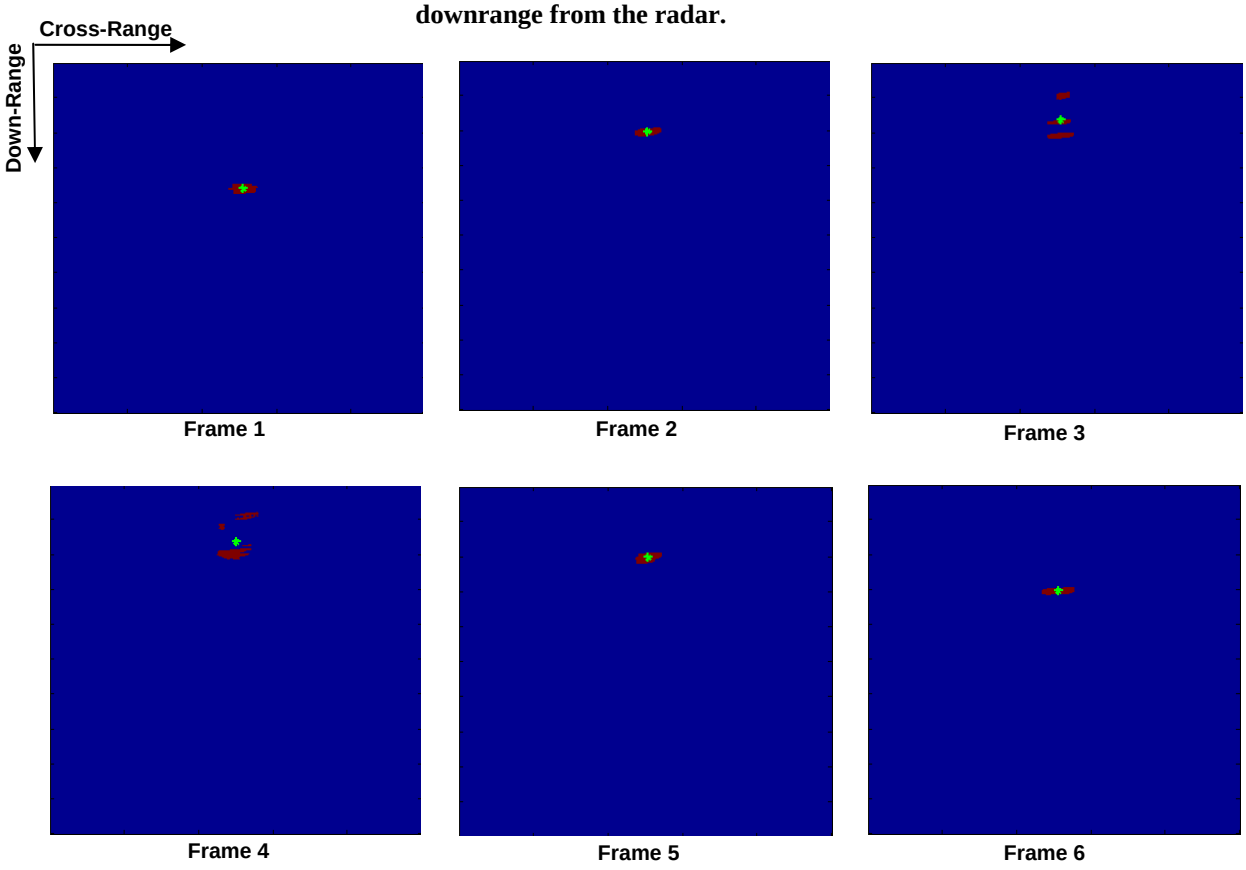


**(b) FAR and clustering algorithm output for Scenario 4. Red diamonds represent POI locations, green cross represent centroid estimates.**

Figure 23. Photos and frames for Scenario 5: the man enters the room (Frames 1 and 2), sits down in the chair, fidgets a while (Frames 3 and 4), and then stands and exits the room (Frames 5 and 6).

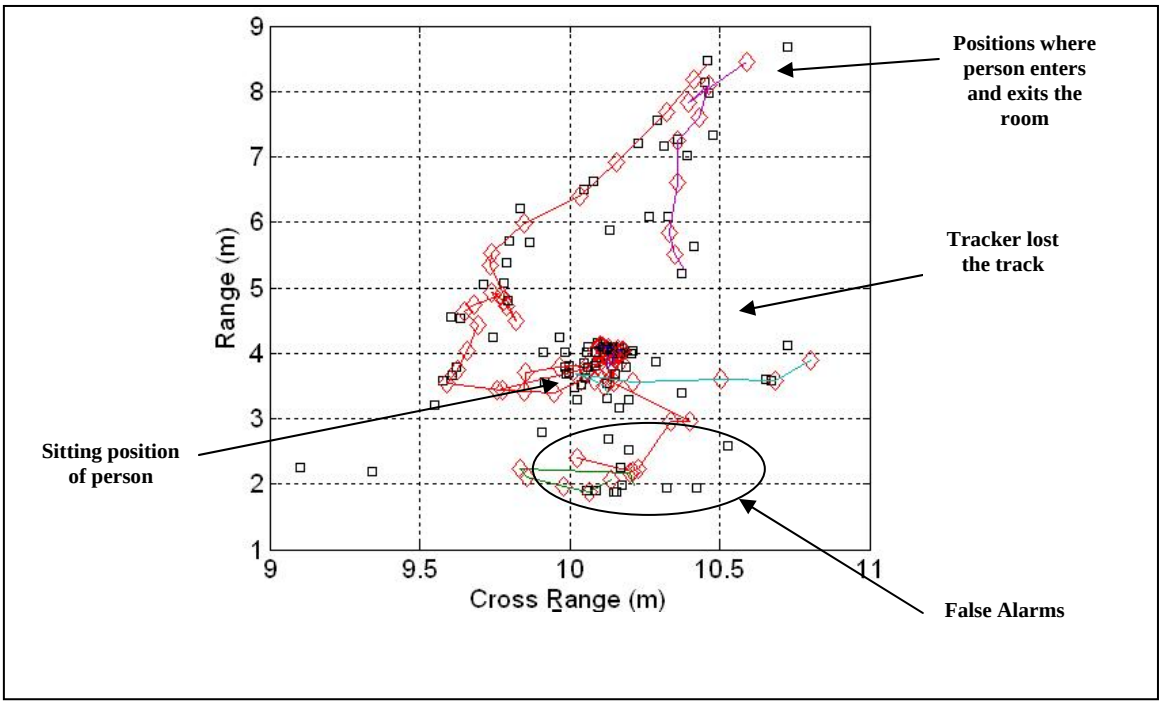


Figure 24. Tracker output of the person walking into a room, sitting in a chair, and leaving the room. The black squares are the positions of the centroids, the red diamonds are the positions estimated by the tracker, and the red line is the estimated path of the moving person output by the tracker.

## 4. Conclusions

We demonstrated the effectiveness of a time-domain MTI processing formulation for detecting moving personnel inside both wood and cinderblock structures, moving personnel walking in nonlinear trajectories, and multiple moving personnel walking in linear trajectories. During MTI operation, the SIRE system remained stationary and collected data from an area under surveillance. This data was then coherently processed in the time domain and change detection was used to indicate the position of the mover relative to the radar in both downrange and cross-range. In addition to the signature of the moving target, the change detection images also contained various image artifacts. For instance, “ghosts” appeared along the back wall due to the shadow from the moving man, and target sidelobes spread target energy in cross-range within the change detection image. The appearance of “ghosts” along the back wall can be eliminated by first generating a SAR image of the building’s layout detailing the locations of the walls; then, any moving target indicated by change detection located along the walls can be removed. Eliminating many of the false alarms due to target sidelobes, however, required implementation of a sophisticated ATD algorithm.

We described such an ATD suite comprising CFAR and clustering algorithms. The ATD algorithms refined the change detection image and eliminated many of the image artifacts; although they did not eliminate all potential false alarms. The tracker algorithm provided a means for eliminating additional false alarms and estimate the path followed by a possible target. We demonstrated how, under certain operating conditions, the tracker was able to maintain the target track while effectively removing false alarms that deviated from the projected target track. It should be noted that we observed this performance when the target followed a circular (i.e., nonlinear) trajectory. Similarly pleasing results were obtained for the case when a target walked to a chair in the center of the room, sat down, fidgeted, and then walked out of the room. These results indicate that our time-domain MTI processing formulation can identify moving targets even when they move slowly along trajectories that are not favorable for classical, Doppler-based MTI.

## 5. References


1. Skolnik, M. *Introduction to Radar Systems*. McGraw-Hill: New York, NY, 2001.

2. Novak, L. Change Detection for Multi-polarization, Nulti-pass SAR. *Proceedings of the SPIE Conference on Algorithms for Synthetic Aperture Radar Imagery XII*, vol. 5808, Orlando, FL, March 2005, 234–246.

3. Ressler, M.; Nguyen, L.; Koenig, F.; Wong, D.; Smith, D. G. The Army Research Laboratory (ARL) Synchronous Impulse Reconstruction (SIRE) Forward-Looking Radar. *Proceedings of the SPIE Conference on Unmanned Systems Technology IX*, vol. 6561, Bellingham, WA, April 2007, 656105-1 – 656105–12.

4. Nguyen, L.; Wong, D.; Ressler, M.; Koenig, F.; Stanton, B.; Smith, G.; Sichina, J.; Kappra, K. Obstacle Avoidance and Concealed Target Detection Using the Army Research Lab Ultra-Wideband Synchronous Impulse Reconstruction (UWB SIRE) Forward Imaging Radar. *Proceedings of the SPIE Conference on Detection and Remediation Technologies for Mines and Minelike Targets XII*, vol. 6553, Bellingham, WA, April 2007, 65530H-1 – 65530H-8.

5. Ranney, K.; Martone, A.; Nguyen, L.; et al. Recent MTI Experiments Using ARL's Synchronous Impulse Reconstruction (SIRE) Radar. *Proceedings of the SPIE conference on Radar Sensor Technology XII*, vol. 6947, Orlando, FL, April 2008.

6. McCorkle, J. Focusing of Synthetic Aperture Ultra Wideband Data. *Proceedings of the IEEE International Conference on Systems Engineering*, Dayton, OH, Aug 1991, 1–5.

7. Farwell, M.; Ross, J.; Lutrell, R.; Cohen, D.; Chin, W.; Dogaru, T. Sense Through the Wall System Development and Design Considerations. *J. of the Franklin Institute* **Sept 2008,** *345* (6), 570–591.

8. Nguyen, L. *Image Resolution Computation for Ultra-Wideband (UWB) Synchronous Impulse Reconstruction (SIRE) Radar*; ARL-TN-0294; U.S. Army Research Laboratory: Adelphi, MD, July 2007.

9. Gandhi, P. P.; Kassam, S. A. Analysis of CFAR Processors in Homogeneous Background. *IEEE Transactions on Aerospace and Electronic Systems* **July 1988**, *24* (4), 427–445.

10. Wilpon, J.; Rabiner, L. A Modified K-means Clustering Algorithm for Use in Isolated Work Recognition. *IEEE Transactions on Acoustics, Speech and Signal Processing* **July 1985**, *33* (3), 587–594.

11. MacQueen, J. Some Methods for Classification and Analysis of Multivariate Observations. *Proceedings of the 5th Berkeley Symposium on Probability and Statistics*, vol. *1*, Berkeley, CA, 1967, 281–296.

12. Duta, R.; Hart, P.; Stork, D. *Pattern Classification*; 2nd ed., John Wiley and Sons Inc.: New York, NY, 2001.

13. Thorndike, R. Who Belongs in the Family? *Psychometrika* **Dec 1953**, *18* (4), 267–276.

14. Zhao, Q.; Xu, M.; Franti, P. Knee Point Detection on Bayesian Information Criteria. *Proceedings of the 20th IEEE International Conference on Tools with Artificial Intelligence*, vol. 2, Nov 2008, 431-438.

15. Blackman, S.; Popoli, R. *Design and Analysis of Modern Tracking Systems*; Artech House: Norwood, MA, 1999.

## List of Symbols, Abbreviations, and Acronyms

| | |
|---|---|
| ARL | U.S. Army Research Laboratory |
| ATD | automatic target detection |
| CD | change detection |
| CFAR | constant false alarm rate |
| MT | moving target |
| MTI | moving-target detection |
| NMSOS | normalized minimized SOS |
| POIs | points of interest |
| SAR | synthetic-aperture-radar |
| SIRE | Synchronous Impulse Reconstructive |
| SNR | signal-to-noise ratio |
| SOS | sum of squares |
| STTW | sensing through the wall |
| UWB | ultra-wideband |

| No. of Copies | Organization |
|---|---|
| 1 | ADMNSTR<br>ELECT DEFNS TECHL INFO CTR<br>ATTN DTIC OCP (ELECTRONIC COPY)<br>18725 JOHN J KINGMAN RD STE 0944<br>FT BELVOIR VA 22060-6218 |
| 1 | DARPA<br>ATTN IXO S WELBY<br>3701 N FAIRFAX DR<br>ARLINGTON VA 22203-1714 |
| 1 CD | OFC OF THE SECY OF DEFNS<br>ATTN ODDRE (R&AT)<br>THE PENTAGON<br>WASHINGTON DC 20301-3080 |
| 1 | US ARMY RSRCH DEV AND ENGRG CMND<br>ARMAMENT RSRCH DEV AND ENGRG CTR<br>ARMAMENT ENGRG AND TECHNLGY CTR<br>ATTN AMSRD AAR AEF T J MATTS<br>BLDG 305<br>ABERDEEN PROVING GROUND MD 21005-5001 |
| 1 | PM TIMS, PROFILER (MMS-P)<br>AN/TMQ-52<br>ATTN B GRIFFIES<br>BUILDING 563<br>FT MONMOUTH NJ 07703 |
| 1 | US ARMY INFO SYS ENGRG CMND<br>ATTN AMSEL IE TD F JENIA<br>FT HUACHUCA AZ 85613-5300 |
| 1 | COMMANDER<br>S ARMY RDECOM<br>TTN AMSRD AMR W C MCCORKLE<br>400 FOWLER RD<br>EDSTONE ARSENAL AL 35898-5000 |
| 1 | US GOVERNMENT PRINT OFF<br>DEPOSITORY RECEIVING SECTION<br>ATTN MAIL STOP IDAD J TATE<br>732 NORTH CAPITOL ST NW<br>WASHINGTON DC 20402 |

| No. of Copies | Organization |
|---|---|
| 1 | US ARMY RSRCH LAB<br>ATTN AMSRD ARL CI OK TP<br>T LANDFRIED<br>BLDG 4600<br>ABERDEEN PROVING GROUND MD 21005-5066 |
| 1 | DIRECTOR<br>US ARMY RSRCH LAB<br>ATTN AMSRD ARL RO EV W D BACH<br>PO BOX 12211<br>RESEARCH TRIANGLE PARK NC 27709 |
| 23 | US ARMY RSRCH LAB<br>ATTN AMSRD ARL CI OK PE TECHL PUB<br>ATTN AMSRD ARL CI OK TL TECHL LIB<br>ATTN AMSRD ARL SE RU A MARTONE (10 COPIES)<br>ATTN AMSRD ARL SE RU A SULLIVAN<br>ATTN AMSRD ARL SE RU G SMITH<br>ATTN AMSRD ARL SE RU K KAPPRA<br>ATTN AMSRD ARL SE RU K RANNEY<br>ATTN AMSRD ARL SE RU K SHERBONDY<br>ATTN AMSRD ARL SE RU L NGUYEN<br>ATTN AMSRD ARL SE RU M RESSLER<br>ATTN AMSRD ARL SE RU R INNOCENTI<br>ATTN AMSRD ARL SE RU T DOGARU<br>ATTN AMSRD-ARL-SE-RU J COSTANZA<br>ATTN IMNE ALC HRR MAIL & RECORDS MGMT<br>ADELPHI MD 20783-1198 |
| TOTAL: | 33 (31 HCs, 1 CD, 1 PDF) |